Error Probability and Capacity Analysis of Generalised Pre-coding Aided Spatial Modulation

Rong Zhang, Lie-Liang Yang and Lajos Hanzo
Communications, Signal Processing and Control, School of ECS, University of Southampton, SO17 1BJ, UK
Email: rz,lly,lh@ecs.soton.ac.uk, http://www-mobile.ecs.soton.ac.uk

***Abstract*—The recently proposed Multiple Input Multiple Output (MIMO) transmission scheme termed as Generalised Pre-coding aided Spatial Modulation (GPSM) is analysed, where the key idea is that a particular subset of *receive* antennas is activated and the specific activation pattern itself conveys useful implicit information. We provide the upper bound of both the Symbol Error Ratio (SER) and Bit Error Ratio (BER) expression of the GPSM scheme of a low-complexity decoupled detector. Furthermore, the corresponding Discrete-input Continuous-output Memoryless Channel (DCMC) capacity as well as the achievable rate is quantified. Our analytical SER and BER upper bound expressions are confirmed to be tight by our numerical results. We also show that our GPSM scheme constitutes a flexible MIMO arrangement and there is always a beneficial configuration for our GPSM scheme that offers the same bandwidth efficiency as that of its conventional MIMO counterpart at a lower Signal to Noise Ratio (SNR) per bit.**

I. Introduction

Multiple Input Multiple Output (MIMO) systems constitute one of the most promising recent technical advances in wireless communications, since they facilitate high-throughput transmissions in the context of various standards [1]. Hence, they attracted substantial research interests, leading to the Vertical-Bell Laboratories Layered Space-Time (V-BLAST) scheme [2] and to the classic Space Time Block Coding (STBC) arrangement [3]. The point-to-point single-user MIMO systems are capable of offering diverse transmission functionalities in terms of multiplexing-diversity-and beamforming gains. Similarly, Spatial Division Multiple Access (SDMA) employed in the uplink and multi-user MIMO techniques invoked in the downlink also constitute beneficial building blocks [4], [5]. The basic benefits of MIMOs have also been recently exploited in the context of the network MIMO concept [6], [7], for constructing large-scale MIMOs [8], [9] and for conceiving beneficial arrangements for interference-limited MIMO scenarios [10].

Despite having a plethora of studies on classic MIMO systems, their practical constraints, such as their I/Q imbalance, their transmitter and receiver complexity as well as the cost of their multiple Radio Frequency (RF) Power Amplifier (PA) chains as well as their Digital-Analogue / Analogue-Digital (DA/AD) converters have received limited attention. To circumvent these problems, low complexity alternatives to conventional MIMO transmission schemes have also been proposed, such as the Antenna Selection (AS) [11], [12] and the Spatial Modulation (SM) [13], [14] philosophies. More specifically, SM and generalised SM [15] constitute novel MIMO techniques, which were conceived for providing a higher throughput than a single-antenna aided system, while maintaining both a lower complexity and a lower cost than the conventional MIMOs, since they may rely on a reduced number of RF up-conversion chains. To elaborate a little further, SM conveys extra information by mapping $\log_2(N_t)$ bits to the *Transmit* Antenna (TA) indices of the N_t TAs, in addition to the classic modulation schemes, as detailed in [13].

By contrast, the family of Pre-coding aided Spatial Modulation (PSM) schemes is capable of conveying extra information by appropriately selecting the *Receive* Antenna (RA) indices, as detailed in [16]. More explicitly, in PSM the indices of the RA represent additional information in the spatial domain. As a specific counterpart of the original SM, PSM benefits from both a low cost and a low complexity at the receiver side, therefore it may be considered to be eminently suitable for downlink transmissions [16]. The further improved concept of Generalised PSM (GPSM) was proposed in [17], where comprehensive performance comparisons were carried out between the GPSM scheme as well as the conventional MIMO scheme and the associated detection complexity issues were discussed. Furthermore, a range of practical issues were investigated, namely the detrimental effects of realistic imperfect Channel State Information at the Transmitter (CSIT), followed by a low-rank approximation invoked for large-dimensional MIMOs. Finally, the main difference between our GPSM scheme and the classic SM is that the former requires downlink pre-processing and CSIT, although they may be considered as a dual counterpart of each other and may hence be used in a hybrid manner. Other efforts on robust PSM was reported in [18].

As a further development, in this paper, *we provide the theoretical analysis of the recently proposed GPSM scheme [17], which is not available in the literature. More explicitly, both the Discrete-input Continuous-output Memoryless Channel (DCMC) capacity as well as the achievable rate are characterized. Importantly, tight upper bounds of the Symbol Error Ratio (SER) and Bit Error Ratio (BER) expressions are derived, when a decoupled low-complexity detector is employed.*

The rest of our paper is organised as follows. In Section II, we introduce the underlying concept as well as the detection

The financial support of the EPSRC under the India-UK Advanced Technology Centre (IU-ATC), that of the EU under the Concerto project as well as that of the European Research Council's (ERC) Advanced Fellow Grant is gratefully acknowledged.

methods of the GPSM scheme. This is followed by our analytical study in Section III, where both the DCMC capacity and the achievable rate as well as the SER/BER expressions are derived. Our simulation results are provided in Section IV, while we conclude in Section V.

II. System Model

A. Conceptual Description

Consider a MIMO system equipped with N_t TAs and N_r RAs, where we assume $N_t \geq N_r$. In this MIMO set-up, a maximum of N_r parallel data streams may be supported, conveying a total of $k_{eff} = N_r k_{mod}$ bits altogether, where $k_{mod} = \log_2(M)$ denotes the number of bits per symbol of a conventional M-ary PSK/QAM scheme and its alphabet is denoted by $\mathcal{A}$. Transmitter Pre-Coding (TPC) relying on the TPC matrix of $\boldsymbol{P} \in \mathbb{C}^{N_t \times N_r}$ may be used for pre-processing the source signal before its transmission upon exploiting the knowledge of the CSIT.

In contrast to the above-mentioned classic multiplexing of N_r data streams, in our GPSM scheme a total of $N_a < N_r$ RAs are activated so as to facilitate the simultaneous transmission of N_a data streams, where the particular *pattern* of the N_a RAs activated conveys extra information in form of so-called spatial symbols in addition to the information carried by the conventional modulated symbols. Hence, the number of bits in GPSM conveyed by a spatial symbol becomes $k_{ant} = \lfloor \log_2(|\mathcal{C}_t|) \rfloor$, where the set $\mathcal{C}_t$ contains all the combinations associated with choosing N_a activated RAs out of N_r RAs. As a result, the total number of bits transmitted by the GPSM scheme is $k_{eff} = k_{ant} + N_a k_{mod}$. Finally, it is plausible that the conventional MIMO scheme obeys $N_a = N_r$. For assisting further discussions, we also let $\mathcal{C}(k)$ and $\mathcal{C}(k,i)$ denote the kth RA activation pattern and the ith activated RA in the kth activation pattern, respectively.

B. GPSM Transmitter

More specifically, let $\boldsymbol{s}_m^k$ be an *explicit* representation of a so-called super-symbol $\boldsymbol{s} \in \mathbb{C}^{N_r \times 1}$, indicating that the RA pattern k is activated and N_a conventional modulated symbols $\boldsymbol{b}_m = [b_{m_1}, \ldots, b_{m_{N_a}}]^T \in \mathbb{C}^{N_a \times 1}$ are transmitted, where we have $b_{m_i} \in \mathcal{A}$ and $\mathbb{E}[|b_{m_i}|^2] = 1, \forall i \in [1, N_a]$. In other words, we have the relationship

$$\boldsymbol{s}_m^k = \boldsymbol{\Omega}_k \boldsymbol{b}_m, \tag{1}$$

where $\boldsymbol{\Omega}_k = \boldsymbol{I}[:, \mathcal{C}(k)]$ is constituted by the specifically selected columns determined by $\mathcal{C}(k)$ of an identity matrix of $\boldsymbol{I}_{N_r}$. Following TPC, the resultant transmit signal $\boldsymbol{x} \in \mathbb{C}^{N_t \times 1}$ may be written as

$$\boldsymbol{x} = \sqrt{\beta/N_a} \boldsymbol{P} \boldsymbol{s}_m^k. \tag{2}$$

In order to avoid dramatic power fluctuation during the pre-processing, we introduce the scaling factor of β designed for maintaining either the loose power-constraint of $\mathbb{E}[||\boldsymbol{x}||^2] = 1$ or the strict power-constraint of $||\boldsymbol{x}||^2 = 1$, which are thus denoted by β_l and β_s, respectively.

As a natural design, the TPC matrix has to ensure that no energy leaks into the unintended RA patterns. Hence, the classic linear Channel Inversion (CI)-based TPC [19], [20] may be used, which is formulated as

$$\boldsymbol{P} = \boldsymbol{H}^H (\boldsymbol{H}\boldsymbol{H}^H)^{-1}, \tag{3}$$

where the power-normalisation factor of the output power after pre-processing is given by

$$\beta_l = N_r / \mathrm{Tr}[(\boldsymbol{H}\boldsymbol{H}^H)^{-1}], \tag{4}$$

$$\beta_s = N_a / \boldsymbol{s}^H (\boldsymbol{H}\boldsymbol{H}^H)^{-1} \boldsymbol{s}. \tag{5}$$

The stringent power-constraint of (5) is less common than the loose power-constraint of (4). The former prevents any of the power fluctuations at the transmitter, which was also considered in [19]. For completeness, we include both power-constraints in this paper.

C. GPSM Receiver

The signal observed at the N_r RAs may be written as

$$\boldsymbol{y} = \sqrt{\beta/N_a} \boldsymbol{H} \boldsymbol{P} \boldsymbol{s}_m^k + \boldsymbol{w}, \tag{6}$$

where $\boldsymbol{w} \in \mathbb{C}^{N_r \times 1}$ is the circularly symmetric complex Gaussian noise vector with each entry having a zero mean and a variance of σ^2, i.e. we have $\mathbb{E}[||\boldsymbol{w}||^2] = \sigma^2 \boldsymbol{I}_{N_r}$, while $\boldsymbol{H} \in \mathbb{C}^{N_r \times N_t}$ represents the MIMO channel involved. We assume furthermore that each entry of $\boldsymbol{H}$ undergoes frequency-flat Rayleigh fading and it is uncorrelated between different super-symbol transmissions, while remains constant within the duration of a super-symbol's transmission. The super-symbols transmitted are statistically independent from the noise.

At the receiver, the joint detection of both the conventional modulated symbols $\boldsymbol{b}_m$ and of the spatial symbol k obeys the Maximum Likelihood (ML) criterion, which is formulated as

$$[\hat{m}_1, \ldots, \hat{m}_{N_a}, \hat{k}] = \arg \min_{\boldsymbol{s}_n^\ell \in \mathcal{B}} \{||\boldsymbol{y} - \sqrt{\beta/N_a} \boldsymbol{H} \boldsymbol{P} \boldsymbol{s}_n^\ell||^2\}, \tag{7}$$

where $\mathcal{B} = \mathcal{C} \times \mathcal{A}^{N_a}$ is the joint search space of the super-symbol $\boldsymbol{s}_n^\ell$. Alternatively, decoupled or separate detection may also be employed, which treats the detection of the conventional modulated symbols $\boldsymbol{b}_m$ and the spatial symbol k separately. In this reduced-complexity variant [1], we have

$$\hat{k} = \arg \max_{\ell \in [1, |\mathcal{C}|]} \{\sum_{i=1}^{N_a} |y_{\mathcal{C}(\ell,i)}|^2\}, \tag{8}$$

$$\hat{m}_i = \arg \min_{n_i \in [1,M]} \{|y_{\hat{v}_i} - \sqrt{\beta/N_a} \boldsymbol{h}_{\hat{v}_i} \boldsymbol{p}_{\hat{v}_i} b_{n_i}|^2\}_{\hat{v}_i = \mathcal{C}(\hat{k},i)}, \tag{9}$$

where $\boldsymbol{h}_{\hat{v}_i}$ is the $\hat{v}_i$th row of $\boldsymbol{H}$ representing the channel between the $\hat{v}_i$th RA and the transmitter, while $\boldsymbol{p}_{\hat{v}_i}$ is the $\hat{v}_i$th

[1]The reduced complexity receiver operates in a decoupled manner, which is beneficial in the scenario considered, where the spatial symbols and the conventionally modulated symbols are independent. However, this assumption may not be ideal, when correlations exist between the spatial symbols and the conventionally modulated symbols. In this case, an iterative detection exchanging extrinsic soft-information between the spatial symbols and conventionally modulated symbols may be invoked. Importantly, the iterations would exploit the beneficial effects of improving the soft-information by taking channel decoding into account as well for simultaneously exploiting the underlying correlations, which is reminiscent of the detection of correlated source. A further inspiration would be to beneficially map the symbols to both the spatial and to the conventional domain at the transmitter, so that the benefits of unequal protection could be exploited.

column of $\boldsymbol{P}$ representing the $\hat{v}_i$th TPC vector. Thus, correct detection is declared, when we have $\hat{k} = k$ and $\hat{m}_i = m_i, \forall i$.

Remarks: Note that the complexity of the ML detection of (7) is quite high, which is on the order determined by the super-alphabet $\mathcal{B}$, hence obeying $\mathcal{O}(|\mathcal{C}|M^{N_a})$. By contrast, the decoupled detection of (8) and (9) facilitates a substantially reduced complexity compared to that of (7). More explicitly, the complexity is imposed by detecting N_a conventional modulated symbols, plus the complexity (κ) imposed by the comparisons invoked for non-coherently detecting the spatial symbol of (8), which may be written as $\mathcal{O}(N_a M + \kappa)$. Further discussions about the detection complexity of the decoupled detection of the GPSM scheme may be found in [17], where the main conclusion is that the complexity of the decoupled detection of the GPSM scheme is no higher than that of the conventional MIMO scheme corresponding to $N_a = N_r$.

III. Performance Analysis

We continue by investigating the DCMC capacity of our GPSM scheme, when the joint detection scheme of (7) is used and then quantify its achievable rate, when the realistic decoupled detection of (8) and (9) is employed. The achievable rate expression requires the theoretical BER/SER analysis of the GPSM scheme, which provides more insights into the inner nature of our GPSM scheme [2].

A. DCMC Capacity and Achievable Rate

Both Shannon's channel capacity and its MIMO generalisation are maximized, when the input signal obeys a Gaussian distribution [22]. Our GPSM scheme is special in the sense that the spatial symbol conveys integer values constituted by the RA pattern index, which does not obey the shaping requirements of Gaussian signalling. This implies that the channel capacity of the GPSM scheme depends on a mixture of a continuous and a discrete input. Hence, for simplicity's sake, we discuss the DCMC capacity and the achievable rate of our GPSM scheme in the context of discrete-input signalling for both the spatial symbol and for the conventional modulated symbols mapped to it.

1) DCMC Capacity: Upon recalling the received signal observed at the N_r RAs expressed in (6), the conditional probability of receiving $\boldsymbol{y}$ given that a $\mathcal{M} = |\mathcal{C}|M^{N_a}$-ary super-symbol $\boldsymbol{s}_\tau \in \mathcal{B}$ was transmitted over Rayleigh channel and subjected to the TPC of (3) is formulated as

$$p(\boldsymbol{y}|\boldsymbol{s}_\tau) = \frac{1}{\pi\sigma^2} \exp\left\{\frac{-||\boldsymbol{y} - \boldsymbol{G}\boldsymbol{s}_\tau||^2}{\sigma^2}\right\}, \tag{10}$$

where $\boldsymbol{G} = \sqrt{\beta/N_a}\boldsymbol{H}\boldsymbol{P}$. The DCMC capacity of the ML-based joint detection of our GPSM scheme is given by [23]

$$C = \max_{p(\boldsymbol{s}_1),\ldots,p(\boldsymbol{s}_\mathcal{M})} \sum_{\tau=1}^{\mathcal{M}} \int_{-\infty}^{\infty} p(\boldsymbol{y}, \boldsymbol{s}_\tau) \log_2 \left(\frac{p(\boldsymbol{y}|\boldsymbol{s}_\tau)}{\sum_{\epsilon=1}^{\mathcal{M}} p(\boldsymbol{y}, \boldsymbol{s}_\epsilon)}\right) d\boldsymbol{y}, \tag{11}$$

which is maximized, when we have $p(\boldsymbol{s}_\tau) = 1/\mathcal{M}, \forall\tau$ [23]. Furthermore, we have

$$\begin{aligned}
&\log_2\left(\frac{p(\boldsymbol{y}|\boldsymbol{s}_\tau)}{\sum_{\epsilon=1}^{\mathcal{M}} p(\boldsymbol{y}, \boldsymbol{s}_\epsilon)}\right) = \log_2\left(\frac{p(\boldsymbol{y}|\boldsymbol{s}_\tau)}{\sum_{\epsilon=1}^{\mathcal{M}} p(\boldsymbol{y}|\boldsymbol{s}_\epsilon)p(\boldsymbol{s}_\epsilon)}\right) \\
&= -\log_2\left(\frac{1}{\mathcal{M}}\sum_{\epsilon=1}^{\mathcal{M}} \frac{p(\boldsymbol{y}|\boldsymbol{s}_\epsilon)}{p(\boldsymbol{y}|\boldsymbol{s}_\tau)}\right) \\
&= \log_2(\mathcal{M}) - \log_2 \sum_{\epsilon=1}^{\mathcal{M}} \exp(\Psi),
\end{aligned} \tag{12}$$

where substituting (10) into (12), the term Ψ is expressed as

$$\Psi = \frac{-||\boldsymbol{G}(\boldsymbol{s}_\tau - \boldsymbol{s}_\epsilon) + \boldsymbol{w}||^2 + ||\boldsymbol{w}||^2}{\sigma^2}. \tag{13}$$

Finally, by substituting (12) into (11) and exploiting that $p(\boldsymbol{s}_\tau) = 1/\mathcal{M}, \forall\tau$, we have

$$C = \log_2(\mathcal{M}) - \frac{1}{\mathcal{M}}\sum_{\tau=1}^{\mathcal{M}} \mathbb{E}_{\boldsymbol{G},\boldsymbol{w}}\left[\log_2 \sum_{\epsilon=1}^{\mathcal{M}} \exp(\Psi)\right]. \tag{14}$$

2) Achievable Rate: The above DCMC capacity expression implicitly relies on the ML-based joint detection of (7), which has a complexity on the order of $\mathcal{O}(\mathcal{M})$. When the reduced-complexity decoupled detection of (8) and (9) is employed, we estimate the achievable rate based on the mutual information $I(z;\hat{z})$ per bit measured for our GPSM scheme between the input bits $z \in [0,1]$ and the corresponding demodulated output bits $\hat{z} \in [0,1]$.

The mutual information per bit $I(z;\hat{z})$ is given for the Binary Symmetric Channel (BSC) by [22]:

$$I(z;\hat{z}) = H(z) - H(z|\hat{z}), \tag{15}$$

where $H(z) = -\sum_z P_z \log_2 P_z$ represents the entropy of the input bits z and P_z is the Probability Mass Function (PMF) of z. It is noted furthermore that we have $H(z) = 1$, when we adopt the common assumption of equal-probability bits, i.e. $P_{z=0} = P_{z=1} = 1/2$. On the other hand, the conditional entropy $H(z|\hat{z})$ represents the average uncertainty about z after observing $\hat{z}$, which is given by:

$$\begin{aligned}
H(z|\hat{z}) &= \sum_{\hat{z}} P_{\hat{z}} \left[\sum_z P_{z|\hat{z}} \log_2 P_{z|\hat{z}}\right] \\
&= -e_\times \log_2 e_\times - (1-e_\times)\log_2(1-e_\times),
\end{aligned} \tag{16}$$

where $e_\times$ is the crossover probability. By substituting (16) into (15) and exploiting $H(z) = 1$ we have:

$$I(z;\hat{z}) = 1 + e_\times \log_2 e_\times + (1-e_\times)\log_2(1-e_\times). \tag{17}$$

Since the input bit in our GPSM scheme may be mapped either to a spatial symbol or to a conventional modulated symbol with a probability of k_{ant}/k_{eff} and $N_a k_{mod}/k_{eff}$, respectively, the achievable rate becomes

$$R = k_{ant} I(e_\times = e^b_{ant}) + N_a k_{mod} I(e_\times = \tilde{e}^b_{mod}), \tag{18}$$

where e^b_{ant} represents the BER of the spatial symbol, while $\tilde{e}^b_{mod}$ represents the BER of the conventional modulated symbols in the *presence* of spatial symbol errors due to the detection of (8).

[2]The Pair-wise Error Probability (PEP) analysis, relying on error events [21], was conducted in our previous contribution for the specific scenario of ML based detection [17]. In this paper, our error probability analysis is dedicated to the low-complexity decoupled detection philosophy

B. Error Probability

1) The expression of e^s_{eff} and e^b_{eff}: Let us first let e^s_{ant} represent the SER of the spatial symbol, while $\tilde{e}^s_{mod}$ represent the SER of the conventional modulated symbols in the *presence* of spatial symbol errors. Let further N^e_{ant} and N^e_{mod} represent the number of symbol errors in the spatial symbols and in the conventional modulated symbols, respectively. Then we have $e^s_{ant} = N^e_{ant}/N_s$ and $\tilde{e}^s_{mod} = N^e_{mod}/N_a N_s$, where N_s is the total number of GPSM symbols. Hence, the average SER e^s_{eff} of our GPSM scheme is given by:

$$\begin{aligned} e^s_{eff} &= (N^e_{ant} + N^e_{mod})/(1+N_a)N_s \\ &= (e^s_{ant} + N_a \tilde{e}^s_{mod})/(1+N_a). \end{aligned} \tag{19}$$

Similarly, the average BER e^b_{eff} of our GPSM scheme may be written as:

$$\begin{aligned} e^b_{eff} &= (k_{ant} e^b_{ant} + N_a k_{mod} \tilde{e}^b_{mod})/k_{eff} \\ &\approx (\delta_{ant} e^s_{ant} + N_a \tilde{e}^s_{mod})/k_{eff}. \end{aligned} \tag{20}$$

where the second equation of (20) follows from the relation

$$\tilde{e}^b_{mod} \approx \tilde{e}^s_{mod}/k_{mod}, \tag{21}$$

$$e^b_{ant} \approx \delta_{k_{ant}} e^s_{ant}/k_{ant}. \tag{22}$$

Importantly, we have Lemma III.1 for the expression of $\delta_{k_{ant}}$ acting as a correction factor in (22).

Lemma III.1. *(Proof in Appendix A) The generic expression of the correction factor $\delta_{k_{ant}}$ for k_{ant} bits of information is given by:*

$$\delta_{k_{ant}} = \delta_{k_{ant}-1} + \frac{2^{k_{ant}-1} - \delta_{k_{ant}-1}}{2^{k_{ant}} - 1}, \tag{23}$$

where given $\delta_0 = 0$, we can recursively determine $\delta_{k_{ant}}$.

Furthermore, by considering (21) and (22), the achievable rate expressed in (18) may be written as

$$R \approx k_{ant} I(\delta_{k_{ant}} e^s_{ant}/k_{ant}) + N_a k_{mod} I(\tilde{e}^s_{mod}/k_{mod}). \tag{24}$$

Hence, as suggested by (19), (20) and (24), we find that both the average error probability as well as the achievable rate of our GPSM scheme requires the entries of e^s_{ant} and $\tilde{e}^s_{mod}$, which will be discussed as follows.

2) Upper bound of e^s_{ant}: We commence our discussion by directly formulating the following lemma:

Lemma III.2. *(Proof in Appendix B) The upper bound of the analytical SER of the spatial symbol of our GPSM scheme relying on CI TPC may be formulated as:*

$$\begin{aligned} e^s_{ant} &\le e^{s,ub}_{ant} \\ &= 1 - \int_0^\infty \left\{ \int_0^\infty [F_{\chi^2_2}(g)]^{N_r - N_a} f_{\chi^2_2}(g;\lambda) dg \right\}^{N_a} f_\lambda(\lambda) d\lambda, \end{aligned} \tag{25}$$

where $F_{\chi^2_2}(g)$ represents the Cumulative Distribution Function (CDF) of a chi-square distribution having two degrees of freedom, while $f_{\chi^2_2}(g;\lambda)$ represents the Probability Distribution Function (PDF) of a non-central chi-square distribution having two degrees of freedom and non-centrality given by

$$\lambda = \beta/N_a\sigma_0^2, \tag{26}$$

with its PDF of $f_\lambda(\lambda)$ and $\sigma_0^2 = \sigma^2/2$. Finally, equality of (25) holds when $N_a = 1$.

Moreover, the PDF of $f_\lambda(\lambda)$ is formulated in Lemma III.3 and Lemma III.4, respectively, when either the loose or stringent power-normalisation factor of (4) and (5) is employed.

Lemma III.3. *(Proof in Appendix C) When CI TPC is employed and the loose power-normalisation factor of (4) is used, the distribution $f_\lambda(\lambda)$ of the non-centrality λ is given by:*

$$f_\lambda(\lambda) = \frac{2N_r}{\lambda^2 N_a \sigma^2} f_{\boldsymbol{U}} \left(\frac{2N_r}{\lambda N_a \sigma^2} \right), \tag{27}$$

where by letting $\boldsymbol{U} = \mathrm{Tr}[(\boldsymbol{H}\boldsymbol{H}^H)^{-1}]$, we have $f_{\boldsymbol{U}}(\cdot)$, which constitutes the derivative of $F_{\boldsymbol{U}}(\cdot)$ and it is given in (50) of Appendix C.

Lemma III.4. *(Proof in Appendix D) When CI TPC is employed and the stringent power-normalisation factor of (5) is used, the distribution $f_\lambda(\lambda)$ of the non-centrality λ is given by:*

$$f_\lambda(\lambda) = \frac{N_a^{N_t - N_r + 1} \sigma^2/2}{(N_t - N_r)!} e^{-\lambda N_a \sigma^2/2} (\lambda \sigma^2/2)^{N_t - N_r}. \tag{28}$$

3) Upper bound of $\tilde{e}^s_{mod}$: Considering a general case of N_r as well as N_a and assuming that the RA pattern $\mathcal{C}(k)$ was activated, after substituting (3) into (6), we have:

$$y_{v_i} = \sqrt{\beta/N_a} b_{m_i} + w_{v_i}, \qquad \forall v_i \in \mathcal{C}(k), \tag{29}$$

$$y_{u_i} = w_{u_i}, \qquad \forall u_i \in \bar{\mathcal{C}}(k), \tag{30}$$

where $\bar{\mathcal{C}}(k)$ denotes the complementary set of the activated RA pattern $\mathcal{C}(k)$ in $\mathcal{C}$. Hence, we have the Signal to Noise Ratio (SNR) given as

$$\gamma = \gamma_{v_i} = \beta/N_a\sigma^2 = \lambda/2, \qquad \forall v_i \tag{31}$$

and for the remaining deactivated RAs in $\bar{\mathcal{C}}(k)$, we have only random noises of zero mean and variance of σ^2.

The SER e^s_{mod} of the conventional modulated symbol $b_{m_i} \in \mathcal{A}$ in the *absence* of spatial symbol errors may be upper bounded by [24]:

$$e^s_{mod} < N_{min} \int_0^\infty \mathcal{Q}\left(d_{min} \sqrt{\gamma/2} \right) f_\gamma(\gamma) d\gamma = e^{s,ub}_{mod}, \tag{32}$$

where in general $f_\gamma(\gamma)$ has to be acquired by the empirical histogram based method. When Lemma III.3 or Lemma III.4 is exploited, $f_\gamma(\gamma)$ is a scaled version of $f_\lambda(\lambda)$, i.e. we have $f_\gamma(\gamma) = 2f_\lambda(2\gamma)$. Moreover, d_{min} is the minimum Euclidean distance in the conventional modulated symbol constellation, N_{min} is the average number of the nearest neighbours separated by d_{min} in the constellation and $\mathcal{Q}(\cdot)$ denotes the Gaussian $\mathcal{Q}$-function.

When taking into account of the spatial symbol errors, we have Lemma III.5 for the upper bound of $\tilde{e}^s_{mod}$.

Lemma III.5. *(Proof in Appendix E) Given the kth activated RA patten, the SER of the conventional modulated symbols in*

the presence of spatial symbol errors can be upper bounded by:

$$\tilde{e}^{s}_{mod} < (1-e^{s,ub}_{ant})e^{s,ub}_{mod} + e^{s,ub}_{ant}\sum_{\ell\neq k}\frac{N_c e^{s,ub}_{mod} + N_d e^{s}_{o}}{N_a(2^{k_{ant}}-1)} = \tilde{e}^{s,ub}_{mod}, \tag{33}$$

where N_c and $N_d = (N_a - N_c)$ represent the number of common and different RA between $\mathcal{C}(\ell)$ and $\mathcal{C}(k)$, respectively. Mathematically we have $N_c = \sum_{i=1}^{N_a}\mathbb{I}\left[\mathcal{C}(\ell,i)\in\mathcal{C}(k)\right]$. Moreover, $e^{s}_{o} = (M-1)/M$ is SER as a result of random guess.

4) Upper bound of e^{s}_{eff} and e^{b}_{eff}: By substituting (25) and (33) into (19) and (20), we arrive at the upper bound of the average symbol and bit error probability as

$$e^{s,ub}_{eff} = (e^{s,ub}_{ant} + N_a\tilde{e}^{s,ub}_{mod})/(1+N_a) \tag{34}$$

$$e^{b,ub}_{eff} = (\delta_{ant}e^{s,ub}_{ant} + N_a\tilde{e}^{s,ub}_{mod})/k_{eff}. \tag{35}$$

Similarly, by substituting (25) and (33) into (24), we obtain the lower bound of the achievable rate as

$$R^{lb} = k_{ant}I\left(\delta_{k_{ant}}\frac{e^{s,ub}_{ant}}{k_{ant}}\right) + N_a k_{mod}I\left(\frac{\tilde{e}^{s,ub}_{mod}}{k_{mod}}\right). \tag{36}$$

IV. Numerical Results

We now provide numerical results for characterizing both the DCMC capacity of our GPSM scheme and for demonstrating the accuracy of our analytical error probability results.

A. DCMC Capacity

1) Effect of the Number of Activated RAs: Fig 1 characterises the DCMC capacity versus the SNR of the CI TPC aided GPSM scheme based on the loose power-normalisation factor of (4) under $\{N_t, N_r\} = \{8, 4\}$ and employing QPSK, while having $N_a = \{1, 2, 3, 4\}$ activated RAs. It can be observed in Fig 1 that the larger N_a, the higher the capacity of our GPSM scheme. Importantly, both the GPSM scheme of $N_a = 3$ marked by the diamonds and its conventional MIMO counterpart of $N_a = 4$ marked by the triangles attain the same ultimate DCMC capacity of 8 bits/symbol at a sufficiently high SNR, albeit the former exhibits a slightly higher capacity before reaching the 8 bits/symbol value. Furthermore, the DCMC capacity of the conventional Maximal Eigen-Beamforming (Max EB) scheme is also included as a benchmark under $\{N_t, N_r\} = \{8, 4\}$ and employing QPSK, which exhibits a higher DCMC capacity at low SNRs, while only supporting 2 bits/symbol at most.

We further investigate the attainable bandwidth efficiency by replacing the SNR used in Fig 1 by the SNR per bit in Fig 2, where we have $\mathrm{SNR_b[dB]} = \mathrm{SNR[dB]} - 10\log_{10}(C/N_a)$. It can be seen from Fig 2 that the lower N_a, the higher the bandwidth efficiency attained in the low range of $\mathrm{SNR_b}$. Importantly, the achievable bandwidth efficiency of $N_a = 3$ is consistently and significantly higher than that achieved by $N_a = 4$, before they both converge to 8 bits/symbol/Hz at their maximum. Overall, there is always a beneficial configuration for our GPSM scheme that offers the same bandwidth efficiency as that of its conventional MIMO counterpart, which is achieved at a lower SNR per bit.

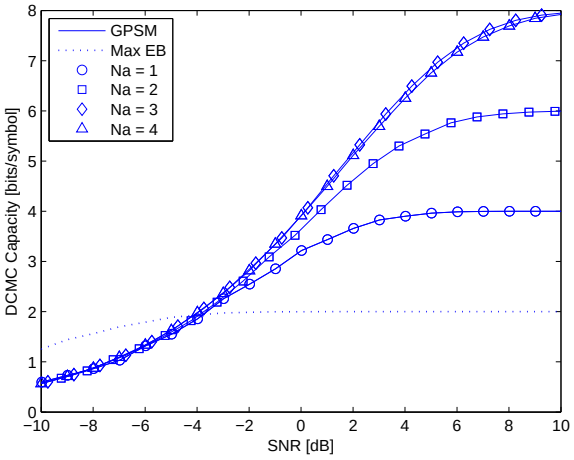

Fig. 1. DCMC capacity versus the SNR of the CI TPC aided GPSM scheme based on the loose power-normalisation factor of (4) under $\{N_t, N_r\} = \{8, 4\}$ and employing QPSK, while having $N_a = \{1, 2, 3, 4\}$ activated RAs.

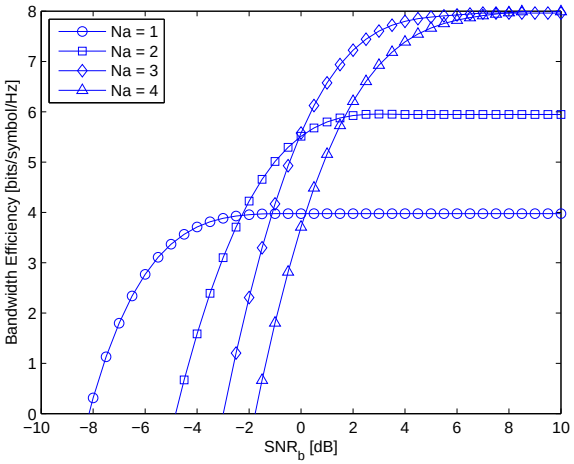

Fig. 2. Bandwidth efficiency versus the $\mathrm{SNR_b}$ of CI TPC aided GPSM scheme with the loose power-normalisation factor of (4) under $\{N_t, N_r\} = \{8, 4\}$ and employing QPSK, while having $N_a = \{1, 2, 3, 4\}$ activated RAs.

2) Robustness to Impairments: Like in all TPC schemes, an important aspect related to GPSM is its resilience to CSIT inaccuracies. In this paper, we let $\boldsymbol{H} = \boldsymbol{H}_a + \boldsymbol{H}_i$, where $\boldsymbol{H}_a$ represents the matrix hosting the average CSI, with each entry obeying the complex Gaussian distribution of $h_a \sim \mathcal{CN}(0, \sigma_a^2)$ and $\boldsymbol{H}_i$ is the instantaneous CSI error matrix obeying the complex Gaussian distribution of $h_i \sim \mathcal{CN}(0, \sigma_i^2)$, where we have $\sigma_a^2 + \sigma_i^2 = 1$. As a result, only $\boldsymbol{H}_a$ is available at the transmitter for pre-processing.

Another typical impairment is antenna correlation. The correlated MIMO channel is modelled by the widely-used Kronecker model, which is written as $\boldsymbol{H} = (\boldsymbol{R}_t^{1/2})\boldsymbol{G}(\boldsymbol{R}_r^{1/2})^T$, with $\boldsymbol{G}$ representing the original MIMO channel imposing no correlation, while $\boldsymbol{R}_t$ and $\boldsymbol{R}_r$ represents the correlations at the transmitter and receiver side, respectively, with the correlation entries given by $R_t(i,j) = \rho_t^{|i-j|}$ and $R_r(i,j) = \rho_r^{|i-j|}$.

Fig 3 and Fig 4 characterise the effect of imperfect CSIT

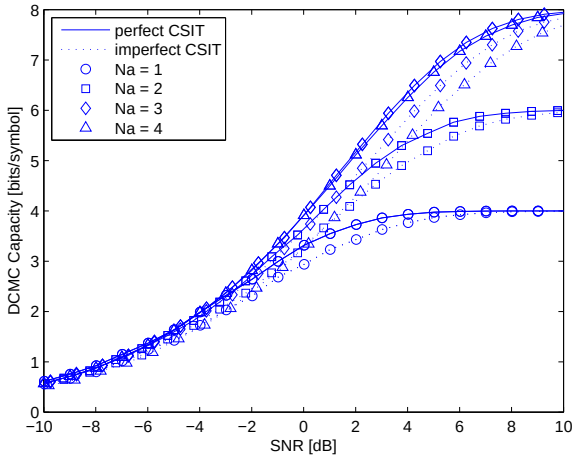

Fig. 3. The effect of imperfect CSIT with $\sigma_i = 0.4$ on the DCMC capacity versus the SNR of CI TPC aided GPSM scheme with the loose power-normalisation factor of (4) under $\{N_t, N_r\} = \{8, 4\}$ and employing QPSK having $N_a = \{1, 2, 3, 4\}$ activated RAs.

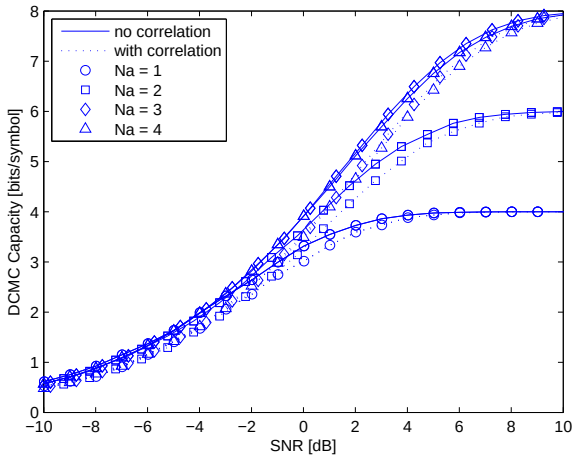

Fig. 4. The effect of antenna correlation with $\rho_t = \rho_r = 0.3$ on the DCMC capacity versus the SNR of CI TPC aided GPSM scheme with the loose power-normalisation factor of (4) under $\{N_t, N_r\} = \{8, 4\}$ and employing QPSK having $N_a = \{1, 2, 3, 4\}$ activated RAs.

associated with $\sigma_i = 0.4$ and of antenna correlation of $\rho_t = \rho_r = 0.3$ on the attainable DCMC capacity versus the SNR for our CI TPC aided GPSM scheme with the loose power-normalisation factor of (4), respectively, under $\{N_t, N_r\} = \{8, 4\}$ and employing QPSK having $N_a = \{1, 2, 3, 4\}$ activated RAs. It can be seen that as expected, both impairments result into a degraded DCMC capacity. Observe in Fig 3 for imperfect CSIT that the degradation of the conventional MIMO associated with $N_a = 4$ and marked by the triangle is larger than that of our GPSM scheme corresponding $N_a = \{1, 2, 3\}$. On the other hand, as seen in Fig 4, roughly the same level of degradation is observed owing to antenna correlation.

3) Effect of Modulation Order and MIMO Configuration: Fig 5 characterises the DCMC capacity versus the SNR of our CI TPC aided GPSM scheme relying on the loose power-

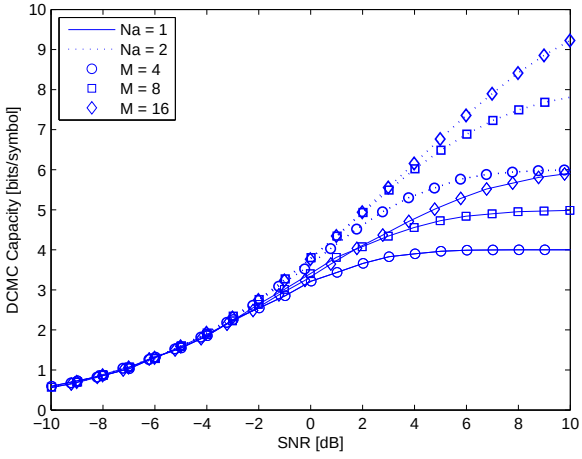

Fig. 5. DCMC capacity versus the SNR of our CI TPC aided GPSM scheme relying on the loose power-normalisation factor of (4) under $\{N_t, N_r\} = \{8, 4\}$ and employing various conventional modulation schemes having $N_a = \{1, 2\}$ activated RAs.

normalisation factor of (4) under $\{N_t, N_r\} = \{8, 4\}$ and employing various conventional modulation schemes having $N_a = \{1, 2\}$ activated RAs. It can be seen that the higher the modulation order M, the higher the achievable DCMC capacity. Furthermore, for a fixed modulation order M, the higher the value of N_a, the higher the achievable DCMC capacity becomes as a result of the information embedded in the spatial symbol.

Fig 6 characterises the DCMC capacity versus the SNR for our CI TPC aided GPSM scheme for the loose power-normalisation factor of (4) under different settings of $\{N_t, N_r\}$ with $N_t/N_r = 2$ and employing QPSK, while having $N_a = \{1, 2\}$ activated RAs. It can be seen in Fig 6 that for a fixed MIMO setting, the higher the value of N_a, the higher the DCMC capacity becomes. Importantly, for a fixed N_a, the larger the size of the MIMO antenna configuration, the higher the DCMC capacity.

B. Achievable Rate

1) Error Probability: Fig 7 - Fig 10 characterize the GPSM scheme's SER as well as the BER under both the loose power-normalisation factor of (4) and the stringent power-normalisation factor of (5) for $\{N_t, N_r\} = \{16, 8\}$ and employing QPSK, respectively. From Fig 7 to Fig 10, we recorded the curves from left to right corresponding to $N_a = \{1, 2, 4, 6\}$. For reasons of space-economy and to avoid crowded figures, our results for $N_a = \{3, 5, 7\}$ were not shown here, but they obey the same trends.

It can be seen from Fig 7 and Fig 9 that our analytical SER results of (34) form tight upper bounds for the empirical simulation results. Hence they are explicitly referred to as 'tight upper bound' in both figures. Additionally, a loose upper bound of the GPSM scheme's SER is also included, which may be written as

$$e_{eff}^{s,lub} = 1 - (1 - e_{ant}^{s,ub})(1 - e_{mod}^{s,ub}). \quad (37)$$

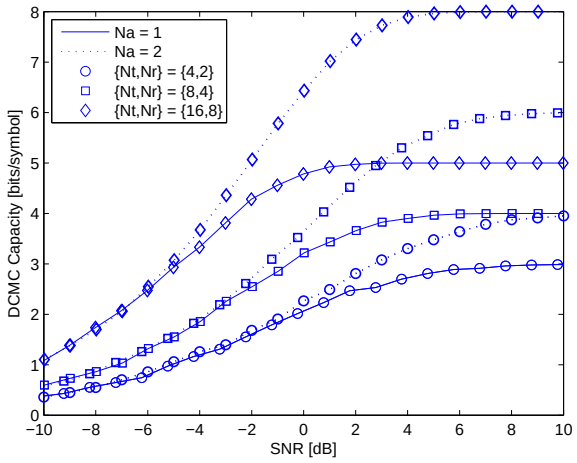

Fig. 6. DCMC capacity versus the SNR for our CI TPC aided GPSM scheme for the loose power-normalisation factor of (4) under different settings of $\{N_t, N_r\}$ with $N_t/N_r = 2$ and employing QPSK, while having $N_a = \{1, 2\}$ activated RAs.

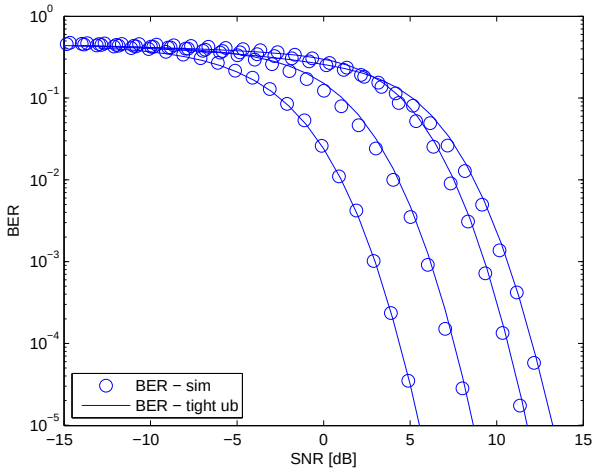

Fig. 8. GPSM scheme's BER with CI TPC and the **loose** power-normalisation factor of (4) under $\{N_t, N_r\} = \{16, 8\}$ and employing QPSK. Curves from left to right correspond to $\{N_a = 1, 2, 4, 6\}$.

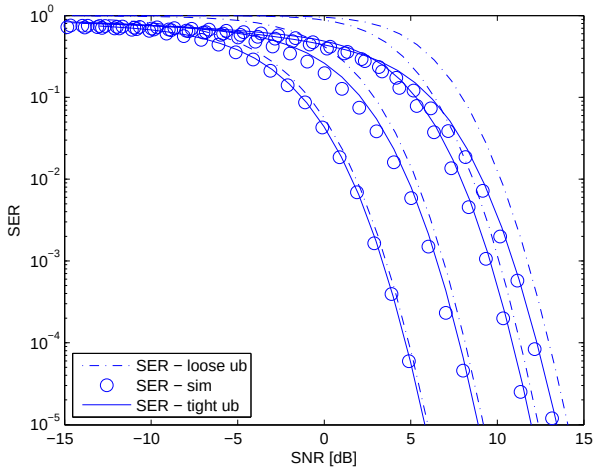

Fig. 7. GPSM scheme's SER with CI TPC and the **loose** power-normalisation factor of (4) under $\{N_t, N_r\} = \{16, 8\}$ and employing QPSK. Curves from left to right correspond to $N_a = \{1, 2, 4, 6\}$.

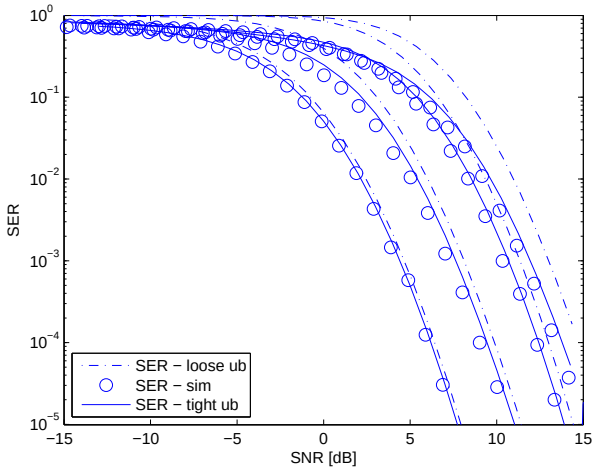

Fig. 9. GPSM scheme's SER with CI TPC and the **stringent** power-normalisation factor of (5) under $\{N_t, N_r\} = \{16, 8\}$ and employing QPSK. Curves from left to right correspond to $N_a = \{1, 2, 4, 6\}$.

Note that in this loose upper bound expression, $e_{mod}^{s,ub}$ of (32) is required rather than $\tilde{e}_{mod}^{s,ub}$ of (33). This expression implicitly assumes that the detection of (8) and (9) are independent. However, the first-step detection of (8) significantly affects the second-step detection of (9). Hence, the loose upper bound shown by the dash-dot line is only tight for $N_a = 1$ and becomes much looser upon increasing N_a, when compared to the tight upper bound of (34).

Similarly, when the GPSM scheme's BER is considered in Fig 8 and Fig 10, our the analytical results of (35) again form tight upper bounds for the empirical results.

2) Separability: To access the inner nature of first-step detection of (8), Fig 11 reveals the separability between the activated RAs and deactivated RAs in our GPSM scheme, where the PDF of (44) and (45) were recorded both for SNR $= -5$ dB (left subplot) and for SNR $= 0$ dB (right subplot) respectively for the same snapshot of MIMO channel realisation with the aid of CI TPC and the loose power-normalisation factor of (4) under $\{N_t, N_r\} = \{16, 8\}$ and employing QPSK. By comparing the left subplot to the right subplot, it becomes clear that the higher the SNR, the better the separability between the activated and the deactivated RAs, since the mean of the solid curves representing (44) move further apart from that of the dashed curve representing (45). Furthermore, as expected, the lower N_a, the better the separability becomes, as demonstrated in both subplots of Fig 11.

3) Comparison: Finally, Fig 12 characterizes the comparison between the DCMC capacity (14) of our GPSM scheme relying implicitly on the ML-based joint detection of (7) and its lower bound of the achievable rate in (36) relying on the low-complexity decoupled detection of (8) and (9), where we use CI TPC with the loose power-normalisation factor of

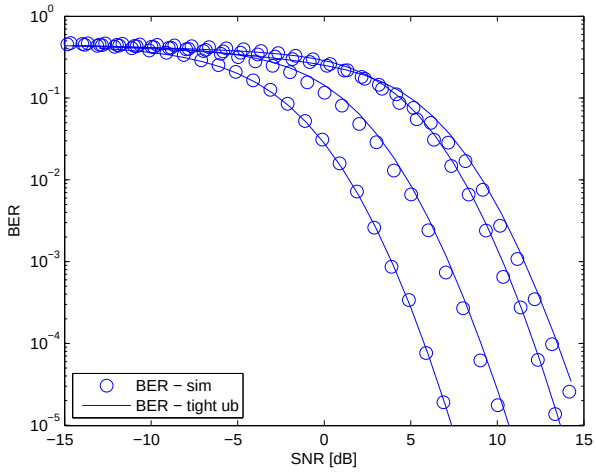

Fig. 10. GPSM scheme's BER with CI TPC and the **stringent** power-normalisation factor of (5) under $\{N_t, N_r\} = \{16, 8\}$ and employing QPSK. Curves from left to right correspond to $\{N_a = 1, 2, 4, 6\}$.

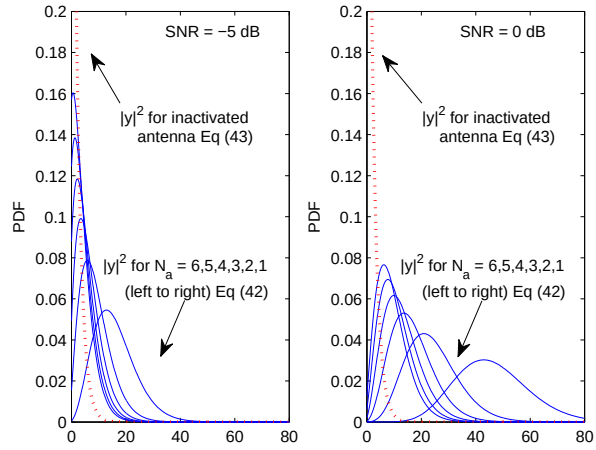

Fig. 11. The PDF of (44) and (45) under both SNR $= -5$ dB (left) and SNR $= 0$ dB (right) for the same snapshot of MIMO channel realisation with CI TPC and the loose power-normalisation factor of (4) under $\{N_t, N_r\} = \{16, 8\}$ and employing QPSK.

(4) under $\{N_t, N_r\} = \{16, 8\}$ and employing QPSK having $N_a = \{1, 2, 3\}$.

It is clear that the DCMC capacity is higher than the achievable rate for each N_a considered, although both of them converge to the same value, when the SNR is sufficiently high. Noticeably, the discrepancy between the two quantities before their convergence is wider, when N_a is higher. This is because the higher N_a, the lower the achievable rate at low SNRs, which is shown by comparing the solid curves. This echoes our observations of Fig 11, namely that a higher N_a leads to a reduced separability and consequently both to a higher overall error probability and to a lower achievable rate. In fact, the achievable rate becomes especially insightful after being compared to the DCMC capacity, where we may tell how a realistic decoupled detection performs and how far its performance is from the DCMC capacity.

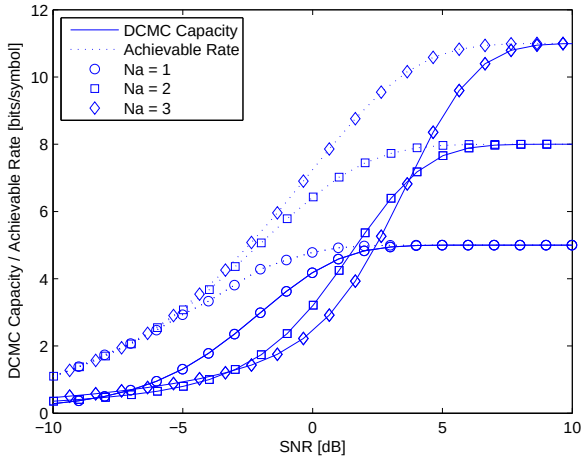

Fig. 12. Comparison between the DCMC capacity of our GPSM scheme relying implicitly on the ML-based joint detection and its lower bound of the achievable rate relying on the low-complexity decoupled detection, where we use CI TPC with the loose power-normalisation factor of (4) under $\{N_t, N_r\} = \{16, 8\}$ and employing QPSK having $N_a = \{1, 2, 3\}$.

V. Conclusions

In this paper, we introduced the concept of our GPSM scheme and carried out its theoretical analysis in terms of both its DCMC capacity as well as its achievable rate relying on our analytical upper bound of the SER and the BER expressions, when a low-complexity decoupled detector is employed. Our numerical results demonstrate that the upper bound introduced is tight and the DCMC capacity analysis indicates that our GPSM scheme constitutes a flexible MIMO arrangement. Our future work will consider a range of other low-complexity MIMO schemes, such as the receive antenna selection and the classic SM, in the context of large-scale MIMOs.

Furthermore, the insights of our error probability and capacity analysis are multi-folds:

- It can be seen that there is a gap between the DCMC capacity relying on ML detection and the achievable rate of decoupled detection. Thus, a novel detection method is desired for closing this gap and for striking a better trade-off between the performance attained and the complexity imposed.
- The error probability derived serves as a tight upper bound of our GPSM performance. This facilitates the convenient study of finding beneficial bit-to-symbol mapping and error-probability balancing between the spatial symbols and conventional modulated symbols [25]. Otherwise, excessive-complexity bit-by-bit Monte-Carlo simulations would be required.
- Furthermore, both the capacity and error probability analysis provide a bench-marker for conducting further research on antenna selection techniques for our GPSM scheme, where different criteria may be adopted either for maximizing the capacity or for minimizing the error probability, again without excessive-complexity bit-by-bit Monte-Carlo simulations.

APPENDIX A
PROOF OF LEMMA III.1

Let $\mathcal{A}_{k_{ant}}$ denote the alphabet of the spatial symbol having k_{ant} bits of information. Then the cardinality of the alphabet $\mathcal{A}_{k_{ant}}$ is twice higher compared to that of $\mathcal{A}_{k_{ant}-1}$. Thus, $\mathcal{A}_{k_{ant}}$ may be constructed by two sub-alphabets of $\mathcal{A}_{k_{ant}-1}$, represented by 0 and 1, respectively. We may thereafter refer to the alphabet of $\mathcal{A}_{k_{ant}-1}$ preceded by the above-mentioned with 0 (1) as zero-alphabet (one-alphabet).

Assuming that the spatial symbol representing k_{ant} zeros was transmitted, we may then calculate the total number of pair-wise bit errors ϵ_0 in the above zero-alphabet. Hence, the number of pair-wise bit errors ϵ_1 in the one-alphabet is simply $\epsilon_1 = \epsilon_0 + A$, where $A = 2^{k_{ant}}$ accounts for the difference in the first preceding bit. Hence the total number of pair-wise bit errors is $\epsilon = 2\epsilon_0 + 2^{k_{ant}}$. Taking into account an equal probability of $1/(2^{k_{ant}} - 1)$ for each possible spatial symbol error, we arrive at the correction factor given by $\delta_{k_{ant}} = (2\epsilon_0 + 2^{k_{ant}})/(2^{k_{ant}} - 1)$.

Since ϵ_0 represents the total number of pair-wise bit errors corresponding to case of $(k_{ant} - 1)$ bits of information, we have $\epsilon_0 = (2^{k_{ant}-1} - 1)\delta_{k_{ant}-1}$. Hence the resultant expression of the correction factor may be calculated recursively according to (23) after some further manipulations[3].

APPENDIX B
PROOF OF LEMMA III.2

Considering a general case of N_r as well as N_a and assuming that the RA pattern $\mathcal{C}(k)$ was activated, after substituting (3) into (6), we have:

$$y_{v_i} = \sqrt{\beta/N_a} b_{m_i} + w_{v_i}, \qquad \forall v_i \in \mathcal{C}(k), \tag{38}$$

$$y_{u_i} = w_{u_i}, \qquad \forall u_i \in \bar{\mathcal{C}}(k), \tag{39}$$

where $\bar{\mathcal{C}}(k)$ denotes the complementary set of the activated RA pattern $\mathcal{C}(k)$ in $\mathcal{C}$. Furthermore, upon introducing $\sigma_0^2 = \sigma^2/2$, we have:

$$|y_{v_i}|^2 = \mathcal{R}(y_{v_i})^2 + \mathcal{I}(y_{v_i})^2 \tag{40}$$

$$\sim \mathcal{N}(\sqrt{\beta/N_a}\mathcal{R}(b_{m_i}), \sigma_0^2) + \mathcal{N}(\sqrt{\beta/N_a}\mathcal{I}(b_{m_i}), \sigma_0^2), \tag{41}$$

$$|y_{u_i}|^2 = \mathcal{R}(w_{u_i})^2 + \mathcal{I}(w_{u_i})^2 \tag{42}$$

$$\sim \mathcal{N}(0, \sigma_0^2) + \mathcal{N}(0, \sigma_0^2), \tag{43}$$

where $\mathcal{R}(\cdot)$ and $\mathcal{I}(\cdot)$ represent the real and imaginary operators, respectively. As a result, by normalisation with respect to σ_0^2, we have the following observations:

$$|y_{v_i}|^2 \sim \chi_2^2(g; \lambda_{v_i}), \qquad \forall v_i \in \mathcal{C}(k), \tag{44}$$

$$|y_{u_i}|^2 \sim \chi_2^2(g), \qquad \forall u_i \in \bar{\mathcal{C}}(k), \tag{45}$$

[3]By assuming equal-probability erroneously detected patterns, a spatial symbol may be mistakenly detected as any of the other spatial symbols with equal probability. Let us now give an example for highlighting the rationale of introducing the correction factor. For example, spatial symbol '0' carrying bits [0,0] was transmitted, it would result into a one-bit difference when the spatial symbol '1' carrying [0,1] or '2' carrying [1,0] was erroneously detected. However, it would result into a two-bits difference when spatial symbol '3' carrying [1,1] was erroneously detected. This corresponds to four bit errors in total for these three cases, thus a correction factor of 4/3 is needed when converting the symbol error ratio to bit error ratio.

where the non-centrality is given by $\lambda_{v_i} = \beta|b_{m_i}|^2/N_a\sigma_0^2$. Exploiting the fact that $\mathbb{E}[|b_{m_i}|^2] = 1, \forall i$ (or $|b_{m_i}|^2 = 1, \forall i$ for PSK modulation), we have $\lambda = \lambda_{v_i}, \forall v_i$. Note that λ is also a random variable obeying the distribution of $f_\lambda(\lambda)$.

Recall from (8) that the correct decision concerning the spatial symbols occurs, when $\sum_{i=1}^{N_a} |y_{v_i}|^2$ is the maximum. By exploiting the fact that $\mathbb{E}_{\mathcal{C}(k)}[\Delta] = \Delta$, the correct detection probability Δ of the spatial symbols given the non-centrality λ, when the RA pattern $\mathcal{C}(k)$ was activated may be lower bounded as in (46). More explicitly,

- equation (a) serves as the lower bound, since it sets the most strict condition for the correct detection, when each metric y_{u_j} of the inactivated RA indices in $\bar{\mathcal{C}}(k)$ is lower than each metric g_{v_i} of the activated RA indices in $\mathcal{C}(k)$. Note that, equality holds when $N_a = 1$;
- equation (b) follows from the fact that the N_a random variables $|y_{v_i}|^2$ are independent of each other;
- equation (c) follows from the fact that the $(N_r - N_a)$ random variables $|y_{u_j}|^2$ are independent and equation (d) follows from the fact that the N_a independent variables of $|y_{v_i}|^2$ and the $(N_r - N_a)$ independent variables of $|y_{u_j}|^2$ are both identically distributed.

As a result, after averaging over the distribution of $f_\lambda(\lambda)$, the analytical SER e_{ant}^s of the spatial symbol in our GPSM scheme may be upper bounded as in (25). In general, the expression of $f_\lambda(\lambda)$ can be acquired with the aid of the empirical histogram based method, while in case the loose / stringent power-normalisation factor of (4) / (5) is used, the analytical expression for $f_\lambda(\lambda)$ is given in Lemma III.3 / Lemma III.4.

APPENDIX C
PROOF OF LEMMA III.3

Upon expanding the expression of λ in (26) by taking into account (4), we have:

$$\lambda = \frac{\beta_l}{N_a\sigma_0^2} = \frac{N_r}{N_a\sigma_0^2 \mathrm{Tr}[(\boldsymbol{H}\boldsymbol{H}^H)^{-1}]}. \tag{47}$$

Consider first the distribution of $\mathrm{Tr}[(\boldsymbol{H}\boldsymbol{H}^H)^{-1}]$ and let $\boldsymbol{W} = \boldsymbol{H}\boldsymbol{H}^H$. Since the entries of $\boldsymbol{H}$ are i.i.d. zero-mean unit-variance complex Gaussian random variables, $\boldsymbol{W}$ obeys a complex Wishart distribution. Hence the joint PDF of its eigenvalues $\{\lambda_{\boldsymbol{W}_i}\}_{i=1}^{N_r}$ is given by [26], [27]

$$f_{\boldsymbol{W}}(\{\lambda_{\boldsymbol{W}_i}\}_{i=1}^{N_r}) = \frac{K^{-1}}{N_r!} \prod_i e^{-\lambda_{\boldsymbol{W}_i}} \lambda_{\boldsymbol{W}_i}^{N_t - N_r} \prod_{i<j} (\lambda_{\boldsymbol{W}_i} - \lambda_{\boldsymbol{W}_j})^2, \tag{48}$$

where K is a normalising factor. Thus for its inverse $\boldsymbol{U} = \boldsymbol{W}^{-1}$, we have

$$f_{\boldsymbol{U}}(\{\lambda_{\boldsymbol{W}_i}\}_{i=1}^{N_r}) = \prod_i \lambda_{\boldsymbol{W}_i}^{-2} f_{\boldsymbol{W}}(\{\lambda_{\boldsymbol{W}_i}^{-1}\}_{i=1}^{N_r}). \tag{49}$$

Furthermore, since $\mathrm{Tr}[\boldsymbol{U}] = \sum \lambda_{\boldsymbol{U}_i}$, where $\{\lambda_{\boldsymbol{U}_i}\}_{i=1}^{N_r}$ is the eigenvalues of $\boldsymbol{U}$, we have the CDF of $\mathrm{Tr}[\boldsymbol{U}]$ given by (50), where $T_1 = T$ and $t_1 = 1/T$, while $\forall j > 1$

$$T_j = T - \sum_{i=1}^{j-1} \lambda_{\boldsymbol{U}_i}, \qquad t_j = 1/(T - \sum_{i=1}^{j-1} \lambda_{\boldsymbol{U}_i}^{-1}).$$

$$\Delta \overset{a}{\geq} \int_0^\infty P(|y_{u_1}|^2 < g_{v_1}, \ldots, |y_{u_{N_r-N_a}}|^2 < g_{v_1}, \ldots, |y_{u_1}|^2 < g_{v_{N_a}}, \ldots, |y_{u_{N_r-N_a}}|^2 < g_{v_{N_a}}) \cdot$$
$$P(|y_{v_1}|^2 = g_{v_1}, \ldots, |y_{v_{N_a}}|^2 = g_{v_{N_a}} | \lambda_{v_1}, \ldots, \lambda_{v_{N_a}}) dg_{v_1} \cdots dg_{v_{N_a}}$$
$$\overset{b}{=} \prod_{i=1}^{N_a} \int_0^\infty P(|y_{u_1}|^2 < g_{v_i}, \ldots, |y_{u_{N_r-N_a}}|^2 < g_{v_i}) P(|y_{v_i}|^2 = g_{v_i} | \lambda_{v_i}) dg_{v_i}$$
$$\overset{c}{=} \prod_{i=1}^{N_a} \int_0^\infty \prod_{u_j \in \bar{\mathcal{C}}(k)} P(|y_{u_j}|^2 < g_{v_i}) P(|y_{v_i}|^2 = g_{v_i} | \lambda_{v_i}) dg_{v_i} \overset{d}{=} \left\{ \int_0^\infty [F_{\chi_2^2}(g)]^{N_r - N_a} f_{\chi_2^2}(g; \lambda) dg \right\}^{N_a} \quad (46)$$

Let $\lambda_0 = 1/\mathrm{Tr}[\boldsymbol{U}]$. Then, from the above analysis we know that the PDF of $f_{\mathrm{Tr}[\boldsymbol{U}]}$ is the derivative of (50). Hence, we may also get the PDF of $f_{\lambda_0}(\lambda_0) = \lambda_0^{-2} f_{\mathrm{Tr}[\boldsymbol{U}]}(\lambda_0^{-1})$. Finally, since $\lambda_0 = \lambda N_a \sigma_0^2 / N_r$, we have $f_\lambda(\lambda) = N_a \sigma_0^2 f_{\lambda_0}(\lambda N_a \sigma_0^2 / N_r) / N_r$. After simple manipulations, we have (27).

Appendix D
Proof of Lemma III.4

Upon expanding the expression of λ in (26) by taking into (5), we have:

$$\lambda = \frac{\beta_s}{N_a \sigma_0^2} = \frac{1}{\sigma_0^2 \boldsymbol{s}^H (\boldsymbol{H}\boldsymbol{H}^H)^{-1} \boldsymbol{s}}. \quad (51)$$

Since the entries of $\boldsymbol{H}$ are i.i.d. zero-mean unit-variance complex Gaussian random variables, $\boldsymbol{H}\boldsymbol{H}^H$ obeys a complex Wishart distribution with N_r dimensions and $2N_t$ degrees of freedom, where we have:

$$\boldsymbol{H}\boldsymbol{H}^H \sim \mathcal{CW}(\Sigma, N_r, 2N_t), \quad (52)$$

with $\Sigma = \frac{1}{2} I_{N_r}$ being the variance. By exploiting proposition 8.9 from [28] and letting $\lambda_0 = [\boldsymbol{s}^H (\boldsymbol{H}\boldsymbol{H}^H)^{-1} \boldsymbol{s}]^{-1}$, we have:

$$\lambda_0 \sim \mathcal{CW}[(\boldsymbol{s}^H \Sigma^{-1} \boldsymbol{s})^{-1}, 1, 2(N_t - N_r + 1)], \quad (53)$$

where $A \sim B$ stands for A follows the distribution of B. According to [28], the above one-dimensional complex-valued Wishart distribution is actually a chi-square distribution with $2(N_t - N_r + 1)$ degrees of freedom and scaling parameter of $(\boldsymbol{s}^H \Sigma^{-1} \boldsymbol{s})^{-1} = 1/2N_a$. Thus, the PDF of λ_0 may be explicitly written as:

$$\begin{aligned} f_{\lambda_0}(\lambda_0) &= f_{\chi^2}[2N_a \lambda_0; 2(N_t - N_r + 1)] \\ &= 2N_a \frac{e^{-\lambda_0 N_a} (2N_a \lambda_0)^{N_t - N_r}}{2^{N_t - N_r + 1} (N_t - N_r)!} \\ &= \frac{N_a^{N_t - N_r + 1} e^{-\lambda_0 N_a} \lambda_0^{N_t - N_r}}{(N_t - N_r)!}. \end{aligned} \quad (54)$$

Finally, since $\lambda_0 = \sigma_0^2 \lambda$, we have $f_\lambda(\lambda) = \sigma_0^2 f_{\lambda_0}(\sigma_0^2 \lambda)$, which is (28).

Appendix E
Proof of Lemma III.5

The SER of $\tilde{e}_{mod}^s$ is constituted by the SER of e_{mod}^s, when the detection of the spatial symbol is correct having a probability of $(1 - e_{ant}^s)$, plus the SER, when the detection of the spatial symbol is erroneous having a probability of e_{ant}^s, which is expressed as

$$\begin{aligned} \tilde{e}_{mod}^s &\overset{a}{=} (1 - e_{ant}^s) e_{mod}^s + e_{ant}^s \sum_{\ell \neq k} P_{k \mapsto \ell} \underbrace{\frac{N_c e_{mod}^s + N_d e_o^s}{N_a}}_{E}, \\ &\overset{b}{<} (1 - e_{ant}^s) e_{mod}^{s,ub} + e_{ant}^s \sum_{\ell \neq k} P_{k \mapsto \ell} \frac{N_c e_{mod}^{s,ub} + N_d e_o^s}{N_a}, \\ &\overset{c}{\leq} (1 - e_{ant}^s) e_{mod}^{s,ub} + \frac{e_{ant}^s}{(2^{k_{ant}} - 1)} \sum_{\ell \neq k} \frac{N_c e_{mod}^{s,ub} + N_d e_o^s}{N_a}, \\ &\overset{d}{\leq} (1 - e_{ant}^{s,ub}) e_{mod}^{s,ub} + e_{ant}^{s,ub} \underbrace{\sum_{\ell \neq k} \frac{N_c e_{mod}^{s,ub} + N_d e_o^s}{N_a (2^{k_{ant}} - 1)}}_{A} = \tilde{e}_{mod}^{s,ub}. \end{aligned}$$

Regarding the second additive term of (a), the true activated RA pattern $\mathcal{C}(k)$ may be erroneously deemed to be any of the other legitimate RA patterns $\mathcal{C}(\ell) \in \mathcal{C}, \ell \neq k$ with a probability of $P_{k \mapsto \ell}$, which we have to average over. As for the calculation of the per-case error rates E, when $\mathcal{C}(k)$ was erroneously detected as a particular $\mathcal{C}(\ell)$, we found that it was constituted by the error rates of e_{mod}^s for those N_c RAs in common (which maybe regarded as being partially correctly detected) and the error rates of e_o^s for those RAs that were exclusively hosted by $\mathcal{C}(\ell)$, but were excluded from $\mathcal{C}(k)$. Furthermore, since only random noise may be received by those N_d RAs in $\mathcal{C}(\ell)$, thus e_o^s simply represents the SER as a result of a random guess, i.e. we have $e_o^s = (M-1)/M$. Let us now provide some further detailed discussions of the relations ranging from (b) to (d):

- relation (b) holds true, since $\tilde{e}_{mod}^s$ is a monotonic function of e_{mod}^s, thus it is upper bounded upon replacing e_{mod}^s by $e_{mod}^{s,ub}$;
- although it is natural that patterns with a higher N_c would be more likely to cause an erroneous detection, we assume an equal probability of $P_{k \mapsto \ell} = 1/(2^{k_p} - 1)$. The equal probability assumption thus puts more weight on the patterns having higher N_d, since we have $e_o^s > e_{mod}^{s,ub}$. This leads to the relation of (c). Note that, equality holds when $N_a = 1$, where $N_c = 0$ and $N_d = 1$;
- replacing e_{ant}^s by $e_{ant}^{s,ub}$ puts more weight on the second additive term of (d), since having $e_o^s > e_{mod}^{s,ub}$ leads to the relation of $A > e_{mod}^{s,ub}$. As a result (d) also holds.

$$F_{\mathrm{Tr}[\boldsymbol{U}]}(T) = \int_0^{T_1}\int_0^{T_2}\cdots\int_0^{T_{N_r}} f_{\boldsymbol{U}}(\{\lambda_{\boldsymbol{U}_i}\}_{i=1}^{N_r})d\lambda_{\boldsymbol{U}_{N_r}}\cdots d\lambda_{\boldsymbol{U}_1} = \int_{t_1}^{\infty}\int_{t_2}^{\infty}\cdots\int_{t_{N_r}}^{\infty} f_{\boldsymbol{W}}(\{\lambda_{\boldsymbol{U}_i}^{-1}\}_{i=1}^{N_r})d\lambda_{\boldsymbol{U}_{N_r}}^{-1}\cdots d\lambda_{\boldsymbol{U}_1}^{-1} \quad (50)$$

Again, equality holds when $N_a = 1$, where $e_{ant}^{s} = e_{ant}^{s,ub}$ as indicated by Lemma III.2.

REFERENCES

[1] R. Zhang and L. Hanzo, "Wireless cellular networks," *IEEE Vehicular Technology Magazine*, vol. 5, no. 4, pp. 31–39, 2010.

[2] P. Wolniansky, G. Foschini, G. Golden, and R. Valenzuela, "V-BLAST: an architecture for realizing very high data rates over the rich-scattering wireless channel," in *1998 URSI International Symposium on Signals, Systems, and Electronics*, 1998, pp. 295–300.

[3] S. Alamouti, "A simple transmit diversity technique for wireless communications," *IEEE Journal on Selected Areas in Communications*, vol. 16, no. 8, pp. 1451–1458, 1998.

[4] Q. Spencer, C. Peel, A. Swindlehurst, and M. Haardt, "An introduction to the multi-user MIMO downlink," *IEEE Communications Magazine*, vol. 42, no. 10, pp. 60–67, 2004.

[5] D. Gesbert, M. Kountouris, R. Heath, C.-B. Chae, and T. Salzer, "Shifting the MIMO paradigm," *IEEE Signal Processing Magazine*, vol. 24, no. 5, pp. 36–46, 2007.

[6] H. Zhang and H. Dai, "Cochannel interference mitigation and cooperative processing in downlink multicell multiuser MIMO networks," *EURASIP Journal on Wireless Communications and Networking*, vol. 2004, no. 2, pp. 222–235, 2004.

[7] R. Zhang and L. Hanzo, "Cooperative downlink multicell preprocessing relying on reduced-rate back-haul data exchange," *IEEE Transactions on Vehicular Technology*, vol. 60, no. 2, pp. 539–545, 2011.

[8] T. Marzetta, "Noncooperative cellular wireless with unlimited numbers of base station antennas," *IEEE Transactions on Wireless Communications*, vol. 9, no. 11, pp. 3590–3600, 2010.

[9] F. Rusek, D. Persson, B. K. Lau, E. Larsson, T. Marzetta, O. Edfors, and F. Tufvesson, "Scaling up MIMO: Opportunities and challenges with very large arrays," *IEEE Signal Processing Magazine*, vol. 30, no. 1, pp. 40–60, 2013.

[10] V. Cadambe and S. Jafar, "Interference alignment and degrees of freedom of the K-user interference channel," *IEEE Transactions on Information Theory*, vol. 54, no. 8, pp. 3425–3441, 2008.

[11] A. Molisch and M. Win, "MIMO systems with antenna selection," *IEEE Microwave Magazine*, vol. 5, no. 1, pp. 46–56, 2004.

[12] A. Mohammadi and F. Ghannouchi, "Single RF front-end MIMO transceivers," *IEEE Communications Magazine*, vol. 49, no. 12, pp. 104–109, 2011.

[13] R. Mesleh, H. Haas, S. Sinanovic, C. W. Ahn, and S. Yun, "Spatial modulation," *IEEE Transactions on Vehicular Technology*, vol. 57, no. 4, pp. 2228–2241, 2008.

[14] M. Di Renzo, H. Haas, and P. M. Grant, "Spatial modulation for multiple-antenna wireless systems: a survey," *IEEE Communications Magazine*, vol. 49, no. 12, pp. 182–191, 2011.

[15] J. Wang, S. Jia, and J. Song, "Generalised spatial modulation system with multiple active transmit antennas and low complexity detection scheme," *IEEE Transactions on Wireless Communications*, vol. 11, no. 4, pp. 1605–1615, 2012.

[16] L.-L. Yang, "Transmitter preprocessing aided spatial modulation for multiple-input multiple-output systems," in *IEEE 73rd Vehicular Technology Conference (VTC Spring)*, 2011, pp. 1–5.

[17] R. Zhang, L.-L. Yang, and L. Hanzo, "Generalised pre-coding aided spatial modulation," *IEEE Transactions on Wireless Communications*, vol. 12, no. 11, pp. 5434–5443, 2013.

[18] A. Stavridis, S. Sinanovic, M. D. Renzo, and H. Haas, "Transmit precoding for receive spatial modulation using imperfect channel knowledge," in *IEEE 75th Vehicular Technology Conference (VTC Spring)*, 2012, pp. 1–5.

[19] C. Peel, B. Hochwald, and A. Swindlehurst, "A vector-perturbation technique for near-capacity multiantenna multiuser communication-part I: channel inversion and regularization," *IEEE Transactions on Communications*, vol. 53, no. 1, pp. 195–202, 2005.

[20] Q. Spencer, A. Swindlehurst, and M. Haardt, "Zero-forcing methods for downlink spatial multiplexing in multiuser MIMO channels," *IEEE Transactions on Signal Processing*, vol. 52, no. 2, pp. 461–471, 2004.

[21] M. Di Renzo and H. Haas, "Bit error probability of SM-MIMO over generalized fading channels," *IEEE Transactions on Vehicular Technology*, vol. 61, no. 3, pp. 1124–1144, 2012.

[22] J. A. T. Thomas M. Cover, *Elements of Information Theory*, 2nd ed. Wiley-Interscience, 2006.

[23] R. Gallager, *Information Theory and Reliable Communication*. New York: Wiley, 1968.

[24] M. S. John Proakis, *Digital Communications*, 5th ed. McGraw-Hill Higher Education, 2008.

[25] M. Maleki, H. Bahrami, A. Alizadeh, and N. Tran, "On the performance of spatial modulation: optimal constellation breakdown," *IEEE Transactions on Communications*, vol. 62, no. 1, pp. 144–157, 2014.

[26] E. Telatar, "Capacity of multi-antenna gaussian channels," *European Transactions on Telecommunications*, vol. 10, no. 6, pp. 585–595, 1999.

[27] A. Edelman, *Eigenvalues and Condition Numbers of Random Matrices*. PhD thesis, Department of Mathematics, Massachusetts Institute of Technology, Cambridge, MA, 1989.

[28] M. L. Eaton, *Multivariate Statistics: A Vector Space Approach*. John Wiley & Sons Inc, 1983.

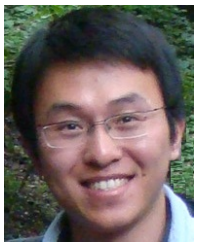

Rong Zhang (M'09) received his PhD (Jun 09) from Southampton University, UK and his BSc (Jun 03) from Southeast University, China. Before doctorate, he was an engineer (Aug 03-July 04) at China Telecom and a research assistant (Jan 06-May 09) at Mobile Virtual Center of Excellence (MVCE), UK. After being a post-doctoral researcher (Aug 09-July 12) at Southampton University, he took industrial consulting leave (Aug 12-Jan 13) for Huawei Sweden R& D as a system algorithms specialist. Since Feb 13, he has been appointed as a lecturer at CSPC group of ECS, Southampton University. He has 30+ journals in prestigious publication avenues (e.g. IEEE, OSA) and many more in major conference proceedings. He regularly serves as reviewer for IEEE transactions/journals and has been several times as TPC member/invited session chair of major conferences. He is the recipient of joint funding of MVCE and EPSRC and is also a visiting researcher under Worldwide University Network (WUN). More details can be found at http://www.ecs.soton.ac.uk/people/rz

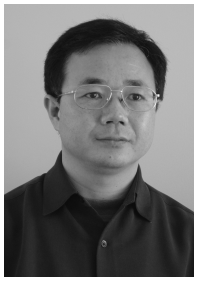

Lie-Liang Yang (M'98, SM'02) received his BEng degree in communications engineering from Shanghai TieDao University, Shanghai, China in 1988, and his MEng and PhD degrees in communications and electronics from Northern (Beijing) Jiaotong University, Beijing, China in 1991 and 1997, respectively. From June 1997 to December 1997 he was a visiting scientist of the Institute of Radio Engineering and Electronics, Academy of Sciences of the Czech Republic. Since December 1997, he has been with the University of Southampton, United Kingdom, where he is the professor of wireless communications in the School of Electronics and

Computer Science. Dr. Yang's research has covered a wide range of topics in wireless communications, networking and signal processing. He has published over 290 research papers in journals and conference proceedings, authored/co-authored three books and also published several book chapters. The details about his publications can be found at http://www-mobile.ecs.soton.ac.uk/lly/. He is a fellow of the IET, served as an associate editor to the *IEEE Trans. on Vehicular Technology* and *Journal of Communications and Networks* (JCN), and is currently an associate editor to the *IEEE Access* and the *Security and Communication Networks (SCN) Journal*.

Lajos Hanzo FREng, FIEEE, FIET, Fellow of EURASIP, DSc received his degree in electronics in 1976 and his doctorate in 1983. In 2009 he was awarded the honorary doctorate "Doctor Honoris Causa" by the Technical University of Budapest. During his 38-year career in telecommunications he has held various research and academic posts in Hungary, Germany and the UK. Since 1986 he has been with the School of Electronics and Computer Science, University of Southampton, UK, where he holds the chair in telecommunications. He has successfully supervised 80+ PhD students, co-authored 20 John Wiley/IEEE Press books on mobile radio communications totalling in excess of 10 000 pages, published 1400+ research entries at IEEE Xplore, acted both as TPC and General Chair of IEEE conferences, presented keynote lectures and has been awarded a number of distinctions. Currently he is directing a 100-strong academic research team, working on a range of research projects in the field of wireless multimedia communications sponsored by industry, the Engineering and Physical Sciences Research Council (EPSRC) UK, the European Research Council's Advanced Fellow Grant and the Royal Society's Wolfson Research Merit Award. He is an enthusiastic supporter of industrial and academic liaison and he offers a range of industrial courses. He is also a Governor of the IEEE VTS. During 2008 - 2012 he was the Editor-in-Chief of the IEEE Press and a Chaired Professor also at Tsinghua University, Beijing. His research is funded by the European Research Council's Senior Research Fellow Grant. For further information on research in progress and associated publications please refer to http://www-mobile.ecs.soton.ac.uk Lajos has 20 000+ citations.